AIP Conference Proceedings

Investigation of structural and optical properties of Ag nanoclusters formed in Si(100) after multiple implantations of low energies Ag ions and post-thermal annealing at a temperature below the Ag-Si eutectic point

Mangal S. Dhoubhadel, Bibhudutta Rout, Wickramaarachchige J. Lakshantha, Sushanta K. Das, Francis D'Souza, Gary A. Glass, and Floyd D. McDaniel

Citation: AIP Conference Proceedings **1607**, 16 (2014); doi: 10.1063/1.4890698
View online: http://dx.doi.org/10.1063/1.4890698
View Table of Contents: http://scitation.aip.org/content/aip/proceeding/aipcp/1607?ver=pdfcov
Published by the AIP Publishing

Articles you may be interested in
Resistive switching characteristics in dielectric/ferroelectric composite devices improved by post-thermal annealing at relatively low temperature
Appl. Phys. Lett. **104**, 092903 (2014); 10.1063/1.4867260

Optical properties and structure characterization of sapphire after Ni ion implantation and annealing
J. Appl. Phys. **98**, 073524 (2005); 10.1063/1.2084314

Scanning tunneling microscopy modification of Ag thin films on Si(100): Local rearrangement of the Si substrate by Ag/Si eutectic phase formation
J. Vac. Sci. Technol. B **15**, 1364 (1997); 10.1116/1.589539

Properties of the TiSi2/p + n structures formed by ion implantation through silicide and rapid thermal annealing
J. Appl. Phys. **72**, 73 (1992); 10.1063/1.352097

Compounds in the Pd-Si and Pt-Si system obtained by electron bombardment and post-thermal annealing
J. Appl. Phys. **52**, 4055 (1981); 10.1063/1.329253

Reuse of AIP Publishing content is subject to the terms at: https://publishing.aip.org/authors/rights-and-permissions IP: 129.120.246.14 On: Wed, 06 Jul 2016 16:41:43

Investigation of structural and optical properties of Ag nanoclusters formed in Si(100) after multiple implantations of low energies Ag ions and post-thermal annealing at a temperature below the Ag-Si eutectic point

Mangal S. Dhoubhadel[1], Bibhudutta Rout[1], Wickramaarachchige J. Lakshantha[1], Sushanta K. Das[2], Francis D'Souza[2], Gary A. Glass[1], Floyd D. McDaniel[1,*]

[1] *Ion Beam Modification and Analysis Laboratory, Department of Physics, University of North Texas, Denton, Texas 76203, USA*

[2] *Department of Chemistry, University of North Texas, Denton, Texas 76203, USA*

Abstract. Multiple low energies (78 keV, 68 keV and 58 keV) of Ag ions with different fluences up to 1×10^{16} atoms/cm^2 were sequentially implanted into Si(100) to create a distribution of different sizes and densities of buried metal nanoclusters (NC) at the near-surface layers. These structures have applications in fields involving plasmonics, optical emitters, photovoltaic, and nano-electronics. The dimension, location and concentration of these NCs influence the type of the applications. The implantation profiles were simulated by utilizing the widely used Stopping and Range of Ions in Matter (SRIM) code as well as a dynamic-TRIM code, which accounts for surface sputtering. The implanted samples were subsequently annealed either in a gas mixture of 4% H_2 + 96% Ar or in vacuum at a temperature ~500 ºC up to 90 minutes. The annealing was carried out below the eutectic temperature (~ 841 ºC) of Ag-Si to preferentially synthesize Ag NCs in Si rather than silicide. In order to study the size, concentration and distribution of the Ag NCs in Si, the samples were characterized by Rutherford Backscattering Spectrometry (RBS), X-ray photoelectron spectroscopy (XPS) in combination with Ar-ion etching, and Transmission Electron Microscopy (TEM) techniques. The annealed samples showed a preferential distribution of the Ag NCs' sizes up to 10 nm either near the surface region (< 25nm) or at deeper layers (60-80 nm) closer to the interface of the implanted layer with the crystalline Si substrate. Ag NCs of larger diameters (up to 15 nm) were seen in the annealed sample near the peak concentration positions (~35-55 nm) of the implanted Ag ions. We have investigated the optical absorption properties due to these nano-structures in Si. The multiple energy implanted samples annealed in a gas mixture of 4% H_2 + 96% Ar show enhancements in the optical absorption in the visible range.

Keywords: Ag nanoclusters, ion implantation, RBS, XPS, TEM.
PACS: 61.80.Jh, 68.35.bg, 68.35.Ct, 68.37.Og, 68.55.Ln
* Corresponding author: mcdaniel@unt.edu

INTRODUCTION

The applications of the transitional metal (e.g. Ag, Au) nanoparticle range from the plasmonics [1-3], photovoltaic device (PV) [4-8], optical antenna, nanoscanning probe [9-12], medical and biosensor [8-9], and nano-drug delivery system [13-14]. The critical factors in influencing the optical and electronic applications of metal nanoparticles are the dimension, location and the density of the nanoparticles [15, 16]. It's been known that in optical applications, the elemental type, size, and shape of a metal nanoparticles or nanoclusters (NC) are correlated to the efficiency and wavelength of the scattering electromagnetic (EM) waves [17]. The visible EM spectrum can penetrate from ~100 nm (for λ=400 nm) to ~7 micrometer (μm) (for λ=700 nm) in crystalline Si (c-Si) and ~100 nm (for λ=400 nm) to ~5 μm (for λ=700 nm) in amorphous Silicon (a-Si) [18].

Ion Beam Synthesis (IBS) involving irradiation of low energy (< 100 keV) metal ions in Si based substrates and subsequent thermal annealing has developed into a reliable technique for production of buried structures in the sub-surface regions (< 60 nm in depth) [19-21]. The ion implantation parameters can control the ion type, fluence (concentration), and the energy (depth); hence one can architect the size and depth of the NP in Si substrate. Since the NCs are formed beneath the top surface, the NCs of implanted materials are well protected; hence the subsequent device can be mechanically robust. As a general rule, the ion implanted NPs are distributed in a more or less Gaussian profile in the ion implanted zone (ion projected range, R_p) in the substrate, but for some materials, there are some preferential sites where the nucleation of NPs are preferable. For example, Au and InP NPs are generally found near the surface, whereas for ZnS NPs are predominantly found at the substrate interface boundary [22].

Radiation Physics
AIP Conf. Proc. 1607, 16-23 (2014); doi: 10.1063/1.4890698
© 2014 AIP Publishing LLC 978-0-7354-1243-9/$30.00

Reuse of AIP Publishing content is subject to the terms at: https://publishing.aip.org/authors/rights-and-permissions IP: 129.120.246.14 On: Wed, 06 Jul 2016 16:41:43

The metallic as well as semiconductor NCs exhibit enhanced optical properties [23]. These optical properties are due to the quantum effects as well as electronic properties influenced by the implanted ion species. The quantum effect is due to the NCs' spatial character such as size, shape, and location. This property enhances the optical properties of the free electrons present in the metallic NCs. Larger NCs are primarily responsible for light absorption and scattering, whereas the smaller NCs are responsible for the nonlinear optical properties. The modified Mie expression [23] in Eq. 1 shows the absorption of light due to the size and ion species of NCs:

$$\alpha = p\frac{18\pi n_d^3}{\lambda}\frac{\varepsilon_2}{(\varepsilon_1+2n_d^2)^2+\varepsilon_2^2} \quad \text{--} \quad \text{Eq. (1),}$$

Where α is the absorption coefficient, p, ε_1, and ε_2 are the volume fraction, real, and imaginary dielectric constant of the NC, respectively, λ is the wavelength of the light, and n_d is the refractive index of the medium.

In this study, we have investigated the synthesis of Ag NCs in Si(100) substrate by implanting multiple energies (< 80 keV) and fluences of Ag ions and subsequent thermal annealing. We report the synthesis, characterization of Ag NCs in Si(100) substrates, surface modification due to the low energy ion irradiation, and optical absorption from the ion irradiation induced modified layers in the Si substrate. The formation and distribution of Ag NCs in Si were characterized by RBS, XPS depth profiling, and TEM techniques. The surface roughness of the Si substrates was characterized by an optical profilometer.

EXPERIMENTAL

Si (100) wafers (Boron doped p-type, resistivity of 10–20 Ωcm) cleaned with acetone were irradiated sequentially with low energies Ag^- ions. The ion energies were 78 keV, 68 keV, and 58 keV with fluences of 1×10^{16} atoms/cm^2, 5×10^{15} atoms/cm^2, and 2.5×10^{15} atoms/cm^2, respectively (designated as type I-sample). To estimate the effects of the irradiation of single energy Ag ions, another set of six samples were created by implanting with single energies of Ag 76 keV, 67 keV, and 57 keV, respectively, and with the two fluences of 5×10^{15} and 1×10^{16} atoms/cm^2. All the samples were tilted to ~5° to the surface normal to avoid ion channeling. The ion implantation source was a National Electrostatic Corporation (NEC) SNICS II (source of negative ion by cesium sputtering), which is one of the three sources attached to NEC 3 MV tandem (9SDH-2 Pelletron) accelerator. The details of the accelerator facility at the Ion Beam Modification and Analysis Laboratory (IBMAL) are provided in reference [24]. The shallow depth ion implantation was carried out in the low energy (LE) implant line of the tandem accelerator [24]. The current density for the ion implantation was maintained at less than one μA/ cm^2 to minimize the self-annealing of the implanted sample. The vacuum of the ion implantation chamber was 1×10^{-6} torr or better. The samples were prepared after simulating the depth profile of the implanted Ag ions in Si according to the Stopping and Range of Ions in Matter (SRIM/TRIM) code [25]. The different energies of Ag ions were implanted in Si (100) in order to have clear ion projected range (Rp) peak separation so that layers of Ag NCs are expected to be formed around the desired depth of Rp. The selection of the ion energy is such that the differences between the R_p are about ~10-30 nm according to the widely used SRIM. We have also used a Dynamic Monte Carlo program or T-DYN based on the static TRIM program [26, 27]. In contrast to the static version, the T-DYN also simulates the dynamic change of surface position due to sputtering and/or deposition of the targets during high fluence ion implantation.

The type-I implanted samples were subsequently annealed in a gas mixture of 4% H_2 + 96% Ar at a temperature ~500 ºC for up to 90 minutes. The annealing was carried out below the eutectic temperature (~ 841 ºC) of Ag-Si to preferentially synthesize Ag NCs in Si rather than silicides. The single energy irradiated samples were annealed in vacuum at a temperature ~500 ºC for up to 90 minutes.

A set of as-implanted and annealed samples were characterized by RBS, XPS, and TEM (for type I only). The RBS measurements were carried out in a NEC 9SH Pelletron accelerator beam line using a rectangular collimated beam of ~1 mm^2 with 2.0 MeV He^+ ions [24]. The solid angle of the RBS (Passivated Implanted Planar Silicon) detector was ~1-2 milli-Sr. at a back scattering angle of 150°. To minimize the secondary electrons, the He^+ ion beam was passes through a series of aperture and ceramic disc magnet just at the opening of the analyzing chamber along with negative 300 volt electron suppressor. The charges were integrated at a tungsten wire mess installed in the beam line right after the slit [28]. A second set of sample were annealed at 500 ^{o}C for 90 minutes. These annealed samples were also characterized using the same techniques as as-implanted samples. The RBS spectra were anlyzed with the SIMNRA computer package [29]. The XPS and TEM measurements were carried out at the Center for Advanced Research and Technology (CART) facility of UNT. The XPS depth profiling measurements were performed with PHI 5000 Versaprobe. Al monochromatic X-ray radiation (1486.6 eV) was focused to a spot size of about 200 μm. The sputtering was performed with a 2 keV Ar beam of 1×1 mm^2 area. The pressure of the target chamber was kept at 7.5×10^{-10} torr.

Reuse of AIP Publishing content is subject to the terms at: https://publishing.aip.org/authors/rights-and-permissions IP: 129.120.246.14 On: Wed, 06 Jul 2016 16:41:43

The TEM measurements were performed using a high resolution FEI Co. Tecnai G2 F20 S-twin machine operated at 200 keV. During the TEM measurement, electron energy loss spectrometry (EELS) of Si and Ag were monitored. The elemental concentration of some of the larger NCs was measured using energy dispersive x-ray (EDX) setup attached to the TEM. The TEM images were analyzed using ImageJ package [30]. The ImageJ is an open source image processing and analysis software package developed by National Institute of Health, USA using the Java program. It can display, edit, and analyze 8–bit, 16–bit, and 32–bit images. The ImageJ package can take input image in many formats including TIFF, GIF, JPEG, BMP, DICOM, FITS, and raw. It is possible to calculate the area and pixel value statistics of user-defined selections in the TEM images. It supports standard image processing functions such as contrast manipulation, sharpening, smoothing, edge detection, and median filtering. It does geometric transformations such as scaling, rotation, and flips. Spatial calibration is available to provide real world dimensional measurements in units such as nanometers. Custom acquisition, analysis, and processing plugins can be developed using ImageJ's built in editor and Java compiler. User-written plugins make it possible to solve many image processing or analysis problem. The image threshold can be selected by choosing one of the several image analysis modes included in the program. We have used the statistical "mean" method for the TEM image analysis. The size selection for the NCs included only from 3 nm^2 to 300 nm^2.

The optical characterization was mainly focused on the specular absorption by the samples. The specular absorption measurement was carried out by using the Shimadzu UV-2550 UV VIS Spectrometers. The spectrometer uses a Halogen Tungsten lamp, which has less than 0.0003% stray light with a 340nm (UV-39) filter. For the specular absorption, a specular reflectance measurement attachment is installed in the spectroscopy instrument. For calibration and setting up the base line absorption spectrum, two identical virgin samples from the same Si wafer are placed on the reference sample holder as well as on the characterizing sample holder. The aperture size for the reference as well as the sample holder was 5 mm diameter. The incident angle of the beam is 5°, which minimizes the influence of polarized light on the absorption spectrum. The base line absorption profile, as well as the normalization of the spectra of the implanted samples with respect to the virgin Si (100) intensity, was automatically adjusted using the UV-2550 spectrometer data acquisition software. Hence the absorption spectrum is the true absorption due to the ion induced modification done on the Si (100) surface layers. Most of the samples were characterized from 900 nm to 200 nm for specular absorption. Optical characterization was done at the Department of Chemistry in UNT.

RESULTS and DISCUSSION

Structural and Compositional Characterization:

In figure 1, simulations of the projected range of the implanted ions for various energies normalized with their respective fluences are presented using the widely used TRIM code as well as the dynamic T-DYN code. In the 'as-implanted' sample, the amorphous layer in Si (a-Si) created by the 78 keV ion implantation was ~85 nm thick. The R_p peaks from the SRIM simulations for 78, 68, and 58 keV Ag ions in Si are 45 nm, 40 nm, 35 nm, respectively, and the peak positions for individual curves are prominently separated from each other. The corresponding T-DYN simulations are shown in solid lines partially overlapping the TRIM simulation. The T-DYN simulations considered the dynamic changes in the target surface layer due to surface sputtering and implantation of the Ag ions. The sum of all the individual energies simulations are also shown to be peaked between ~35-45 nm depth. The corresponding T-DYN simulation for equivalent fluence at 74 keV shows the distribution of the ions is more

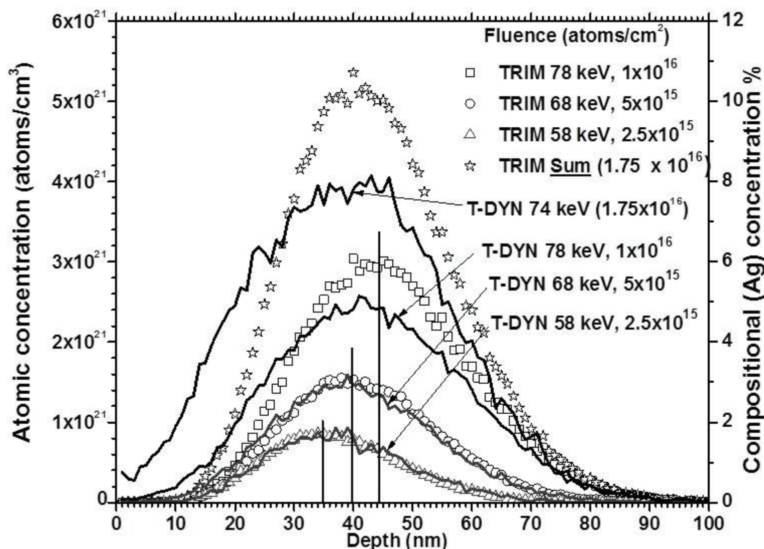

Figure 1. TRIM simulation of the range of various energetic Ag ions in Si normalized with the respective ion fluences. The corresponding Rp values are $Rp_{78\ keV}$ = 45 nm, $Rp_{68\ keV}$ = 40 nm, $Rp_{58\ keV}$ = 35 nm. The corresponding T-DYN simulations are shown in solid lines overlapped with the TRIM plots.

Reuse of AIP Publishing content is subject to the terms at: https://publishing.aip.org/authors/rights-and-permissions IP: 129.120.246.14 On: Wed, 06 Jul 2016 16:41:43

towards the surface region. The T-DYN simulations show the lateral shift in the Rp towards the surface as well as the decrease in the implanted ion concentrations due to the sputtering and redistribution of the surface layers.

In the figure 2, the RBS spectra of the as-implanted and annealed samples are shown for type –I samples (as simulated in figure 1). The RBS spectra simulated by SIMNRA are superimposed on the experimental spectra. The Ag depth profile extracted using the SIMNRA are shown in the inset. The Ag profile of the as-implanted sample agrees quite well with the sum of the T-DYN simulations as shown in figure 1. For the annealed samples, the Ag atoms are seen to have a bimodal distribution, with a component migrating towards the top 20 nm from the surface region and another component centered at ~70 nm from the surface towards the interface of the amorphous and crystalline region of the samples.

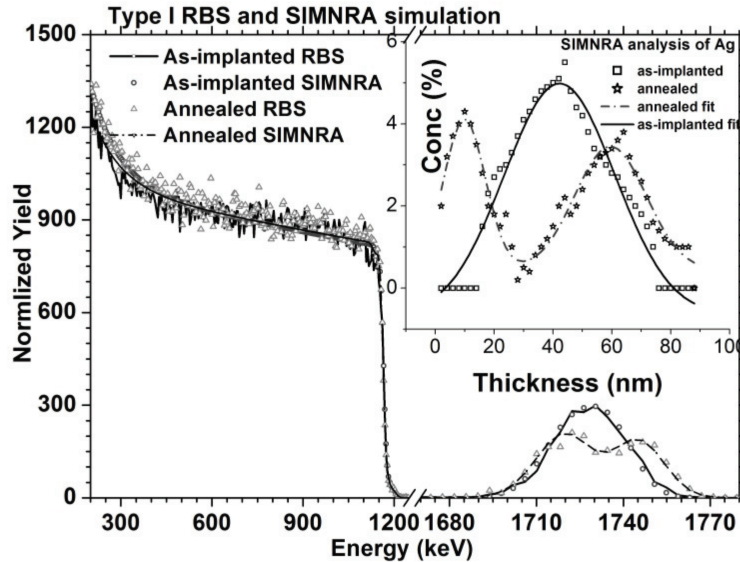

Figure 2. RBS spectra of the as-implanted and annealed Si samples with multiple energy Ag ion implantations (type-I sample). The spectra are overlapped with parameters fitted using the SIMNRA simulation package. The Ag depth profiles extracted using the SIMNRA are shown in the inset for the as-implanted and annealed samples.

In figure 3 the distributions of Ag in the as-implanted and annealed samples for type-I samples are shown using XPS depth profile with Ar ion etching. The general features of the Ag distributions follow the similar trends as the RBS result shown in figure 2. The absolute concentrations of Ag are slightly different in the XPS and RBS results, which may be due to different areas of observation between the two measurements.

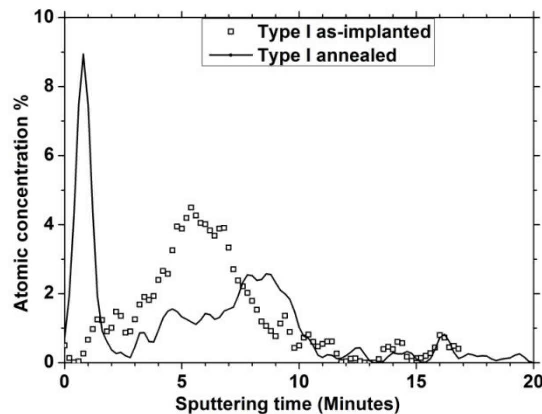

Figure 3. Depth profiles of the Ag in the as-implanted and annealed Si samples (type-I sample) by collecting the Ag (2p) XPS signal from the surfaces while etching the samples using Ar ions.

The TEM images of the as-implanted and annealed Si samples with multiple energy Ag ion implantations (type-I samples) are presented in figure 4. The selected area diffraction (SAD) patterns from the as-implanted region (shown in the inset of the TEM image (Fig. 4(a)), indicates the implanted region (end of the implanted ion range) as totally amorphized Si (a-Si) ~85 nm deep. The SAD patterns from the underlying substrate show the crystalline nature of the Si substrate. In the case of the annealed sample, the TEM image (Fig. 4(b)) shows the shrinkage of a-Si

Reuse of AIP Publishing content is subject to the terms at: https://publishing.aip.org/authors/rights-and-permissions IP: 129.120.246.14 On: Wed, 06 Jul 2016 16:41:43

to ~80 nm and formation of various sizes NCs up to ~15 nm in diameter. Linear profiles using EELS (not shown) across the region containing NCs correspond to the Ag signal from NCs. A similar EDX linear profile across a larger NC (not shown) also indicated the composition of the NC to be Ag. So with these two specific results from EELS and EDX techniques, we assumed all the NCs to be Ag. A detailed image analysis of NCs shown in Fig. 4(b) is presented in Fig. 5 using the ImageJ package [30].

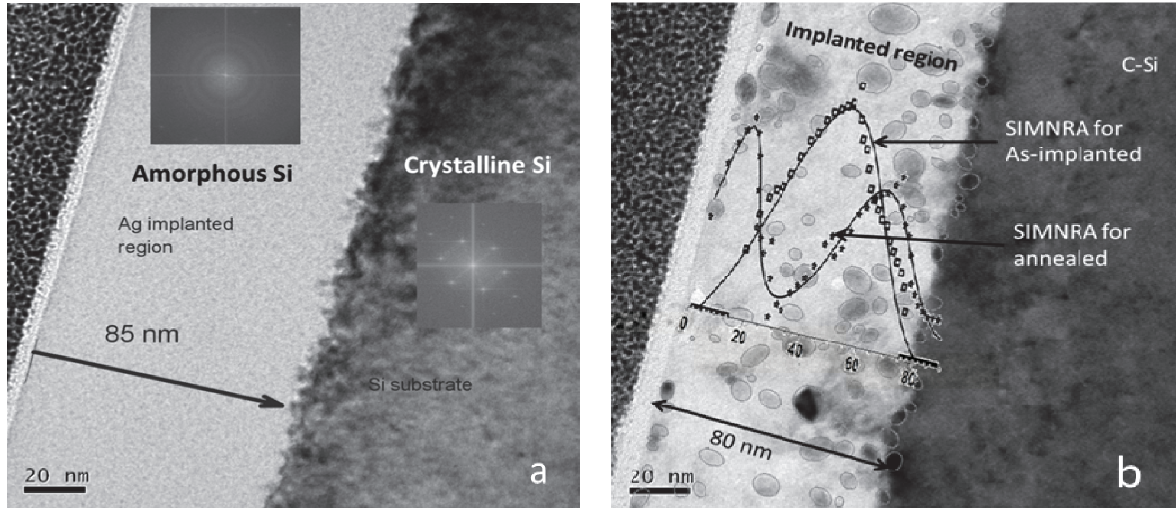

Figure 4. Cross-sectional TEM image of the (a) as-implanted and (b) annealed type-I Ag implanted Si samples. The selected area diffraction (SAD) patterns from the amorphous and crystalline layers are shown in the inset. The Ag implanted region shows the formation of Ag NCs with sizes up to 15 nm (Figure 4b). The encircled areas in the TEM image were used for the analysis of the Ag NCs using imageJ [30]. The corresponding Ag depth profile extracted from the RBS measurements (Fig. 2.) are overlapped in (b).

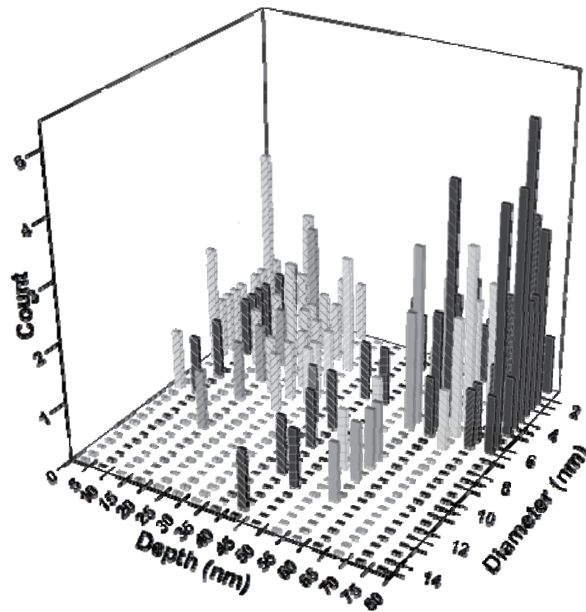

Figure 5. The analysis of the Ag NCs encircled in TEM image (Fig. 4(b)) is presented. The average size of Ag NCs is from ~2 nm to ~15 nm. Ag NCs of larger diameters (up to 15 nm) were seen distributed at the peak concentration positions (~35-55 nm) of the implanted Ag ions.

A multi-dimensional (number of NCs as a function of the depth and size) distribution of NC is presented for the type I sample (Fig. 5). The sizes of the Ag NCs are from ~2 nm to ~15 nm. The areal distribution of smaller Ag NCs in the TEM image has two different preferential regions, one toward the surface region (<25 nm) and another toward the interface of crystalline-Si and amorphous-Si (60-80 nm). Ag NCs of larger diameters (up to 15 nm) were seen

Reuse of AIP Publishing content is subject to the terms at: https://publishing.aip.org/authors/rights-and-permissions IP: 129.120.246.14 On: Wed, 06 Jul 2016 16:41:43

distributed at the peak concentration positions (~35-55 nm) of the implanted Ag ions. These larger NCs were formed due to the availability of higher concentration of the Ag in the peak positions. This distribution of NCs is a significant step in terms of synthesizing layers with tailor made NCs sizes.

Optical Characterization:

The absorption profile of crystalline Si can be enhanced by modifying the Si substrate as well as deposition or implantation of transitional metals in near surface regions. In order to measure and compare the absorption of light by the Si samples modified by ion irradiation; first the absorption of light in the virgin crystalline Si substrate was measured over a range of 200-900 nm wavelengths and normalized to the baseline level (as shown in Fig. 6). The base line Si spectrum shows the virtually flat line absorption. The Si surface and substrate are modified during the ion irradiation. The areal rms value of surface roughness of the virgin Si measured using an optical interference profilometer was found to be less than 0.5 nm whereas, the areal rms roughness value of ion irradiated region was found to be about 0.8 to 1.3 nm. The interaction of visible light on this type of surface roughness act as specular reflection, since the magnitude of visible light wavelength is many orders of magnitude greater than the magnitude of surface roughness.

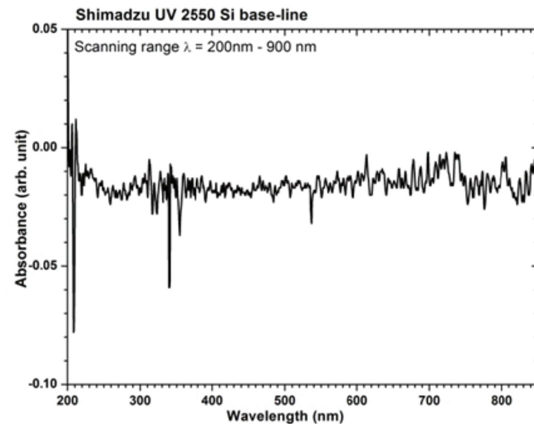

Figure 6. Optical absorption spectrum from a virgin Si substrate.

Figure 7 shows the optical absorption from the multiple energy Ag implanted samples (type-I) for the as-implanted and samples annealed in a gas mixture of 4% H_2 + 96% Ar at a temperature ~500 ºC up to 90 minutes. The relative absorptions of near UV, visible and near IR light with respect to unmodified Si are clearly seen. The UV peaks at 271 nm, 367 nm, and visible peaks at 420 nm, 440 nm and 465 nm, are primarily the defect mitigated absorption further enhanced by the implanted Ag ions. Similar defect oriented absorption in Si has been observed before [30]. The absorptions in the visible to near infrared regions are the direct result due to the shallow depth ion irradiation in the Si. As the ion fluence exceeds a critical range (~5×10^{14} atoms/cm^2 needed to attain full amorphization), the defects induced by the ion irradiation in the Si substrate increases and starts forming clusters of amorphous Si. The amorphized Si has a high density of defects. We have also observed similar absorption in the UV region due to irradiation of low energy (<60 keV) light ions (deuterium, Si) as well as heavy ions (Cu, Au).

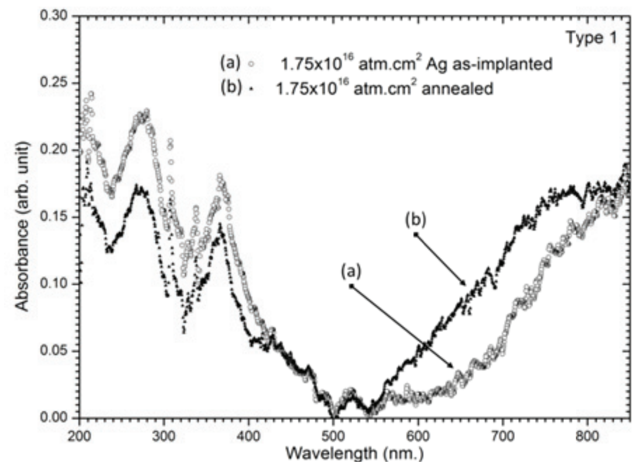

Figure 7. Light absorption profile of 78, 68, and 58 keV Ag implanted (type –I) and annealed sample.

When these ion irradiated samples are thermally annealed, it relaxed the ion induced stress on the surface as well as inside the Si substrate. The thermal annealing produces polycrystalline Si and metallic NCs in the ion induced amorphized Si region. The metal NCs and polycrystalline Si are active optical center [31], which highly interacts with incoming light by absorbing and scattering the light. In the annealed samples (Figure 7), the optical absorption is seen to be enhanced in the visible to infrared region. We believe this enhancement in the optical absorption in the visible range is due to the presence of Ag NCs in the near surface region (top 20 nm) as well as due to the three dimensional distribution of the Ag NCs in the implanted region. One can also see the decrease in the optical absorption in the UV region due to re-ordering/re-crystallization of the top amorphous layers in the Si substrate.

In order to investigate the optical absorption effects of individual components of the multiple energy implanted samples, we have carried out optical measurements on the samples with single energy implants of 76 keV, 67 keV, and 57 keV, respectively, with two different ion fluences of 1×10^{16} and 5×10^{15} atoms/cm^2 separately. Some of these samples were annealed in vacuum at a temperature ~500 ºC up to 90 minutes. In Figure 8, the optical absorption on

Reuse of AIP Publishing content is subject to the terms at: https://publishing.aip.org/authors/rights-and-permissions IP: 129.120.246.14 On: Wed, 06 Jul 2016 16:41:43

the samples implanted with 76 keV Ag ions is shown. Similar to the type-I samples; the absorption in the UV range is seen decreased for the annealed sample. However, the absorption in the visible range is seen slightly decreased as compared to the as-implanted samples. This may be due to the formation of a poly-crystalline Si layers in the top surface and the distribution of Ag NCs in a deeper layer as compared to the multiple energy implanted samples.

Recently Shi et al. have reported better light trapping in double layer Ag NCs sandwiched between SiO_2 layers on solar cells [32]. The multiple energy samples were annealed in a gas mixture of of 4% H_2 + 96% Ar, but there is a possibility of contamination due to the presence of oxygen in the annealing chamber. Though we haven't investigated the presence of oxygen in the top surface layers (~20 nm), we believe the presence of oxygen in the top layers could also make additional contributions besides the Ag NCs to the enhancement in the optical absorption in the visible range replicating similar multilayer structures reported in ref [32].

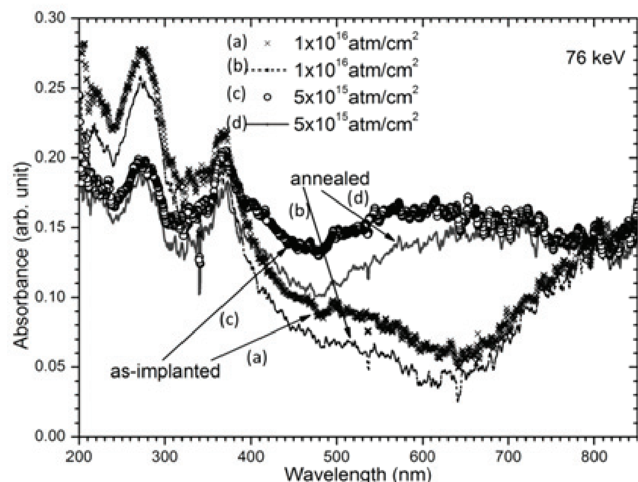

Figure 8. Optical absorption profile of 76 keV Ag as-implanted and annealed in vacuum samples.

CONCLUSIONS

The dimension of scattered EM waves is closely related to the dimension of the NCs. In order to have a broad band of EM waves to interact in a medium, the scattering medium must consist of NCs with a broad range in sizes at the strategic locations. The Ag NCs, implanted with multiple energies and fluences and annealed in a gas mixture of 4% H_2 + 96% Ar at 500 ºC, show the formation of different sizes of NCs. The depth profiles/ distributions of the Ag ions in Si, extracted from RBS and XPS measurements for the as-implanted samples, agrees more with the prediction of the T-DYN simulation for high-fluence implantation. The Ag distribution in the annealed sample shows the preferential locations for the NC formation. All the samples with multi-energy Ag implanted in Si show significant asymmetric diffusion either toward the surface or towards the amorphous/crystalline interface of the substrate. The optical absorption measurement indicate enhancement in the visible range for the annealed samples. Through the distributions of similar size NCs are not well localized, the ion beam synthesis method present a very promising technology to architect NCs localized by their sizes and desirable location.

ACKNOWLEDGEMENTS

The authors would like to thank Dr. Matthias Posselt from the Institute of Ion Beam Physics and Materials Research, Helmholtz-Zentrum Dresden-Rossendorf, Germany for providing the latest version of the T-DYN simulation code. We also like to thank the CART facility at UNT for the use of TEM, XPS characterization equipment. We would like to thank Szabolcs Z. Szilasi at IBMAL, UNT for the help in the measurement of the surface roughness in the samples using an optical profilometer.

REFERENCES

1. Mark. I. Stockman, "Nanoplasmonics: The physics behind the applications", Physics Today, **64**, 2, 24 (2011).
2. M. A. Garcia, "Surface plasmons in metallic nanoparticles: fundamentals and applications", J. Phys. D: Appl. Phys. **44** 283001 (2011).
3. S. Pillai, K. R. Catchpole, T. Trupke, G. Zhang, J. Zhao and M. A. Green, "Enhanced emission from Si-based light-emitting diodes using surface plasmons", Appl. Phys. Lett. **88**, 161102 (2006); doi: 10.1063/1.2195695
4. S. Pillai, K. R. Catchpole, T. Trupke, M. A. Green, Surface plasmon enhanced silicon solar cells, J. Appl. Phys. **101**, 093105 (2007); doi: 10.1063/1.2734885
5. M. A. Green, "The Path to 25% Silicon Solar Cell Efficiency: History of Silicon Cell Evolution", Prog. in Photovoltaics: Res. Appl. **17(3)** 183–189 (2009).
6. Katsuaki Tanabe, Keisuke Nakayama and Harry A. Atwater, "Plasmon-enhanced absorption and photocurrent in ultra-thin GaAs solar cells with metallic nanostructures", *Proc. SPIE* 7047, Nanoscale Photonic and Cell Technologies for Photovoltaics, 704708 (September 11, 2008); http://dx.doi.org/10.1117/12.795469

Reuse of AIP Publishing content is subject to the terms at: https://publishing.aip.org/authors/rights-and-permissions IP: 129.120.246.14 On: Wed, 06 Jul 2016 16:41:43

7. Vivian E. Ferry, Luke A. Sweatlock, Domenico Pacifici, and Harry A. Atwater, "Plasmonic Nanostructure Design for Efficient Light Coupling into Solar Cells", Nano Letters, **8(12)**, 4391-4397, (2008).
8. Louay Eldada, "Nanoscale Self-Assembly of High-Efficiency Copper Indium Gallium Selenide Photovoltaic Thin Films" Proc. SPIE 7402, Nanoengineering: Fabrication, Properties, Optics, and Devices VI, 740206 (25 August 2009); doi: 10.1117/12.827488.
9. U. Kreibig and M. Vollmer, *Optical Properties of Metal Clusters* (Springer, Berlin, 1995).
10. U. Kreigbig, B. Schmitz, and H. D. Breuer, "Separation of plasmon-polariton modes of small metal particles", Phys. Rev. B **36(9)** 5027 (1987).
11. Yanshu Zou, Paul Steinvurzel, Tian Yang, Kenneth B. Crozier, "Surface plasmon resonances of optical antenna atomic force microscope tips" , Appl. Phys. Lett. **94**, 171107 (2009); http://dx.doi.org/10.1063/1.3116145
12. Björn Brian, Borja Sepúlveda, Yury Alaverdyan, Laura M. Lechuga, and Mikael Käll, "Sensitivity enhancement of nanoplasmonic sensors in low refractive index substrates", Optics Express, **17(3)** 2015-2023 (2009) http://dx.doi.org/10.1364/OE.17.002015
13. R. C. Denomme, Z. Young, L. Brock, P. M. Nieva, M. M. Vijayan, "Optimization of a localized surface plasmon resonance biosensor for heat shock protein 70", Proc. of SPIE Vol. **8269**, 82692G (2012).
14. Dan Peer, Jeffrey M. Karp, Seungpyo Hong, Omid C. Farokhzad, Rimona Margalit & Robert Langer, "Nanocarriers as an emerging platform for cancer therapy", Nature Nanotechnology **2**, 751 - 760 (2007).
15. International Technology Roadmap for Semiconductors (ITRS), updated in 2013, http://www.itrs.net/
16. S. Zaima, "Technology Evolution for Silicon Nanoelectronics: Postscaling Technology", Jpn. J. Appl. Phys. **52** 030001 (2013), http://dx.doi.org/10.7567/JJAP.52.030001
17. K. Lance Kelly, Eduardo Coronado, Lin Lin Zhao, and George C. Schatz, "The Optical Properties of Metal Nanoparticles: The Influence of Size, Shape, and Dielectric Environment", J. Phys. Chem. B, **107**, 668-677 (2003).
18. Martin A. Green and Mark J. Keevers "Optical properties of intrinsic silicon at 300 K", Progress in Photovoltaics: Research and Applications, **3(3)** 189-192 (1995), John Wiley & Sons, Ltd.
19. G. Rizza, H. Cheverry, T. Gacoin, A. Lamasson, and S. Henry, "Ion beam irradiation of embedded nanoparticles: Toward an in situ control of size and spatial distribution", J. Appl. Phys. **101**, 014321 (2007); http://dx.doi.org/10.1063/1.2402351
20. P. Kluth, B. Johannessen, G. J. Foran, D. J. Cookson, S. M. Kluth, and M. C. Ridgway, "Disorder and cluster formation during ion irradiation of Au nanoparticles in SiO_2", Phys. Rev. B **74**, 014202 (2006).
21. Feng Ren, Xiang Heng Xiao, Guang Xu Cai, Jian Bo Wang, Chang Zhong Jiang, "Engineering embedded metal nanoparticles with ion beam technology", Appl Phys A **96** 317–325 (2009), DOI 10.1007/s00339-009-5205-3.
22. A. Meldrum, E. Sonder, R. A. Zuhr, I. M. Anderson, J. D. Budai, C. W. White, L. A. Boatner D, O. Henderson, "A transmission electron microscopy investigation of sulfide nanocrystals formed by ion implantation", J. Mater. Res. **14**, 4489 (1999).
23. A. Meldrum, R. Lopez, R. H. Magruder, L. A. Boatner, and C. W. White "Structure and Properties of Nanoparticles Formed by Ion Implantation", Materials Science with Ion Beams, Topics Appl. Physics 116, 255–285 (2010).
24. B. Rout, M. S. Dhoubhadel, P. R. Poudel, V. C. Kummari, B. Pandey, N. T. Deoli, W. J. Lakshantha, S. J. Mulware, J. Baxley, J. E. Manuel, J. L. Pacheco, S. Szilasi, D. L. Weathers, T. Reinert, G. A. Glass, J. L. Duggan, F. D. McDaniel, An Overview of the Facilities, Activities, and Developments at the University of North Texas Ion Beam Modification and Analysis Laboratory (IBMAL), AIP Conference Proceedings, 1544 (2013) 11.
25. J. F. Ziegler, M. D. Ziegler, J. P. Biersack. SRIM – The stopping and range of ions in matter, Nucl. Instr. and Meth. **B268** 1818-1823 (2010), latest version is available at http://www.srim.org/
26. W. Eckstein, J. P. Biersack, Appl. Phys. A 37, 95 (1984); W. Möller, W. Eckstein and J. P. Biersack, Comput. Phys. Commun. 51, 355, (1988). (The permission for the use of the latest version of the TRIDYN package is available at <http://www.hzdr.de/db/Cms?pOid=21578&pNid=0>).
27. Wickramaarachchige J. Lakshantha, Venkata C. Kummari, Tilo Reinert, Floyd D. McDaniel, Bibhudutta Rout, "Depth profile investigation of β-$FeSi_2$ formed in Si(100) by high fluence implantation of 50 keV Fe ion and post-thermal vacuum annealing", Nucl. Inst. And Meth. B (in press). http://dx.doi.org/10.1016/j.nimb.2014.02.024
28. M. E. Bouanani, P. Pelicon, A. Razpet, I. Cadez, M. Budnar, J. Simcic, S. Markelj. Simple and accurate spectra normalization in ion beam analysis using a transmission mesh-based charge integration, Nucl. Instr. and Meth. **B243** 392-396 (2006).
29. An analysis program for RBS analysis, SIMNRA version 6.06 by Matej Mayer. The latest version is available at http://home.rzg.mpg.de/~mam/
30. W. S. Rasband, ImageJ, U. S. National Institutes of Health, Bethesda, Maryland, USA, http://imagej.nih.gov/ij/, 1997-2014.
31. X. L. Wu, S. J. Xiong, G. G. Siu, G. S. Huang, Y. F. Mei, Z. Y. Zhang, S. S. Deng, and C. Tan, "Optical emission from excess Si defect center in Si Nanostructure", Phys. Rev. Letts., **91**, 15 (2003). Yanpeng Shi, Xiaodong Wang, Wen Liu, Tianshu Yang, Rui Xu, and Fuhua Yang, "Multilayer silver nanoparticles for light trapping in thin film solar cells", Jour. of Appl. Physics **113**, 176101 (2013).
32. Yanpeng Shi, Xiaodong Wang, Wen Liu, Tianshu Yang, Rui Xu, and Fuhua Yang, "Multilayer silver nanoparticles for light trapping in thin film solar cells", Jour. of Appl. Physics **113**, 176101 (2013).

Reuse of AIP Publishing content is subject to the terms at: https://publishing.aip.org/authors/rights-and-permissions IP: 129.120.246.14 On: Wed, 06 Jul 2016 16:41:43